



Life-extending Control of Fossil Fuel Power Plants*

P. KALLAPPA,† MICHAEL S. HOLMES† and ASOK RAY†

Optimal feedforward and robust feedback control provides structural durability and desired performance of fossil power plants. Simulation results are presented to demonstrate life extension of a typical power plant while satisfying the performance specifications.

Key Words—Power-station control; feedforward control; robust control.

Abstract—The objective of life-extending control is to achieve a trade-off between structural durability and dynamic performance. This paper focuses on structural durability of the main steam header under load following to illustrate how the life-extending control of fossil fuel power plants can be achieved via feedforward/feedback. This concept is potentially applicable to both new and aging power plants under a variety of operational modes such as hot start-up, scheduled shutdown, and load following where the plant power is rapidly maneuvered to meet the varying load demand. The feedforward control policy is synthesized via nonlinear optimization of a multi-objective cost functional of dynamic performance and service life under the constraints of actuator saturation, operational limitations, and allowable structural damage, including thermomechanical fatigue and plastic deformation. A linear robust feedback control law that is superimposed on the feedforward sequence is synthesized based on induced L_2 -norm techniques. The results of simulation experiments are presented to demonstrate that the proposed feedforward/feedback control policy is potentially capable of ramping the plant power up at a rate of 10% of the full load per minute while maintaining the specified performance and satisfying the damage constraints.
 © 1997 Elsevier Science Ltd.

1. INTRODUCTION

Operation and control procedures for electric power plants require decision-making based on trade off between performance enhancement and life extension (Stultz and Kitto, 1992). Plant performance measure is usually expressed in terms of the thermodynamic efficiency under steady-state operations and matching of actual generated power with the load demand under

transient operations. On the other hand, life extension of a power plant translates into mitigation of structural damage in the critical plant components, for example, due to excessive temperature and pressure oscillations. From these perspectives, the plant performance measure can be modified as a multi-objective cost functional to include the steady-state accuracy, fast dynamic response, availability and structural durability. One obvious benefit of this approach is that service life of critical plant components can be increased with the attendant reduction in the risk of unscheduled shutdown.

Currently, about 45% of the total electric power in the U.S.A. is generated by fossil fuel plants, which, on the average, have a useful service life of about 40 years; and 70% of these plants will be over 30 years old by the year 2000 (Weng, 1994). Under baseload and other steady-state operations, the stress level in the plant components is usually low. However, under transient operating conditions such as start-up, shutdown and load following, the critical plant components are subjected to high thermal and mechanical stresses, and thereby the useful service life is substantially reduced (Stultz and Kitto, 1992). For example, a plant with 40 years of useful life is usually recommended for up to 100 cold starts and shutdowns as an indicator of allowable limits of severe operational transients. Therefore, while matching the varying load demand and keeping the electricity generation cost low, utility companies need to operate these aging power plants under life-extending control to reduce the risk of forced shutdown due to component failures.

This paper introduces and develops a feedforward/feedback methodology for life-extending control of fossil fuel power plants. The objective here is to increase operational

* Received 28 November 1995; revised 6 August 1996; received in final form 7 December 1996. A preliminary version of this paper was presented at the 13th IFAC World Congress, which was held in San Francisco, U.S.A. during 30 June-5 July 1996. The Published Proceedings of this IFAC Meeting may be ordered from: Elsevier Science Limited, The Boulevard, Langford Lane, Kidlington, Oxford OX5 1GB, U.K. This paper was recommended for publication in revised form by Associate Editor M. A. Johnson under the direction of Editor Yaman Arkun. Corresponding author Professor Asok Ray. Tel. +1 814 865 6377; Fax +1 814 863 4848; E-mail axr2@psu.edu.

† Mechanical Engineering Department, The Pennsylvania State University, University Park, PA 16802, U.S.A.

reliability and structural durability without compromising the plant performance under different operating modes. A power plant has many critical components, such as steam generators, main steam and hot reheat steam headers, and main and boiler feedpump turbines and pumps. All these critical components must be taken into consideration in the synthesis of a life-extending control system before its implementation in an operating power plant. To elucidate the underlying principle of life-extending control, this paper focuses on thermomechanical fatigue and creep damage in a specific critical component of fossil fuel power plants, namely the main steam header, which feeds superheated steam from main steam generators into high-pressure turbines. The damage modeling for life extension of other plant components is a subject of current research, and is not reported in this paper.

In general, a combination of feedforward control and feedback control is needed for wide-range operation of fossil power plants (Weng, 1994; Weng and Ray, 1997). The feedforward control policy does not have the ability to compensate for disturbances and noise that may act on the actual plant during its operation. That is, under the feedforward control alone, the plant states may drift away from the desired trajectory. On the other hand, feedback control alone is inadequate for wide range control of the (nonlinear) plant dynamics. These problems can be remedied by feedback control in conjunction with feedforward control. While a robust feedback control law is necessary to overcome modeling uncertainties and perturbations in the system, an open-loop feedforward policy provides the nominal control trajectory that reduces feedback control efforts and improves the overall system performance.

The feedforward part of the control policy is synthesized as a finite sequence of open-loop control inputs via constrained optimization for performance enhancement and life extension specifically under transient conditions. The optimization procedure relies on nonlinear dynamic models, which are formulated based on the physical principles to achieve trade-off between structural durability and dynamic performance. For example, the thermal-hydraulics of the plant dynamics are obtained from conservation of mass, momentum and energy, and thermodynamic state relations (Weng *et al.*, 1996); and the structural-damage model of a critical component is formulated from the principles of fracture mechanics and thermoviscoplasticity (Ray *et al.*, 1994a,b; Dai and Ray, 1995). The linear robust feedback

controller under consideration in this paper, which is synthesized based on induced L_2 -norm techniques (Bamieh and Pearson, 1992), is superimposed on the feedforward control sequence. This feedback controller is implemented in a sampled-data configuration because, like many other practical applications, the continuous-time dynamics of power plants are computer-controlled using sampler and zero-order-hold devices.

The paper is organized in four further sections and an Appendix. Section 2 discusses the plant dynamic model and the structural damage model of the main steam header, which is the critical plant component under consideration in this paper. The governing equations for the structural damage model are derived in the Appendix. Section 3 presents the synthesis of the feedforward/feedback control policy. The results of computer simulation experiments, including the effects of plant dynamic perturbations on performance and damage, are presented in Section 4. Finally, the paper is summarized and concluded in Section 5.

2. MODELING OF PLANT, STRUCTURAL AND DAMAGE DYNAMICS

The damage prediction system, which is an essential ingredient of the life-extending control system, consists of a plant model, structural model(s) of the critical component(s), and the respective damage model(s) as depicted in Fig. 1. The plant model is a finite-dimensional state-space representation of the dynamic process under control. The plant states are inputs to the component structural model, which generates the necessary information for the damage prediction model. The output of the structural model is the *structural stress vector*, which, for example, consists of time-dependent stress, strain and temperature at critical point(s) of the structure (e.g. main steam and hot reheat headers, or superheater and reheater tubes in steam generators). The damage model is a continuous-time representation of material degradation, so that this model can be integrated with the plant dynamic model in the state-variable setting. The objective here is to include the effects of time-dependent damage rate and damage accumulation at the critical points of plant components that are subjected to time-dependent, varying-amplitude load. The damage state vector $v(t)$ indicates the damage levels, for example in terms of fatigue cracks and inelastic strain due to thermomechanical fatigue and creep-plasticity. The time derivative of damage, $\dot{v}(t)$, indicates how the instantaneous load is

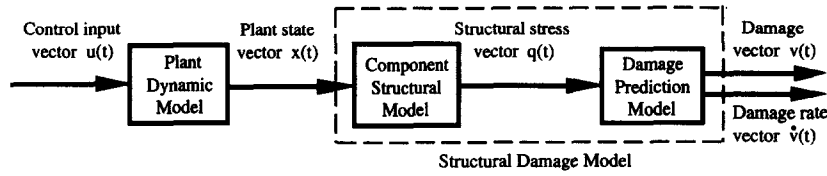


Fig. 1. The damage prediction system.

affecting the critical structure(s) of the plant. The ensemble of the component structural model and the damage prediction model in Fig. 1 is referred to as the structural damage model in the sequel.

The plant dynamics of continuous-time processes and damage dynamics are modeled via nonlinear differential equations, each of which must satisfy the local Lipschitz condition (Vidyasagar, 1992) within the domain of the plant operating range. The plant dynamic model is unaffected by accumulated damage, and hence there is no inherent damage feedback, as seen in Fig. 1. The rationale is that the physical phenomenon of structural damage in a plant component does not alter its macroscopic mechanical behavior (e.g. stiffness constant) within the service life span. An example is fatigue-induced microcracks in a turbine blade that do not alter the natural frequency until the end of its useful life. That is, for a vast majority of cases, when a change in the frequency becomes detectable, the blade life is almost expended. The component structural model and the damage model are derived by applying the fundamental principles of heat transfer, thermodynamics and mechanics to creep and plastic deformation and fatigue crack growth; parameters of these models are dependent on physical dimensions of the critical components and their material properties. The damage model generates both damage rate and accumulation as continuous functions of time. A general structure of the plant and damage dynamics and desired constraints for damage rate and accumulation are represented as follows:

task period: starting time t_0 to final time t_f ;

plant dynamics:

$$\begin{cases} \dot{x} = f(x, u) & \forall t \geq t_0, \text{ given } x(t_0) = x_0, \\ y = g(x, u); \end{cases} \quad (1)$$

damage dynamics: $\dot{v} = h(v, q(x, u))$

$$\text{(such that } h \geq 0 \forall t \geq t_0, \text{ given } v(t_0) = v_0; \quad (2)$$

damage rate tolerance:

$$0 \leq h(v, q(x, u)) < \beta(t) \quad \forall t \in [t_0, t_f]; \quad (3)$$

accumulated damage tolerance:

$$[v(t_f) - v(t_0)] < \Gamma. \quad (4)$$

Here $x \in \mathbb{R}^n$ is the plant state vector, $y \in \mathbb{R}^p$ is

the plant output vector, $u \in \mathbb{R}^m$ is the control input vector, $v \in \mathbb{R}^l$ is the damage state vector, $q \in \mathbb{R}^r$ is the load vector, and $\beta(t) \in \mathbb{R}^l$ and $\Gamma \in \mathbb{R}^l$ are specified tolerances for the damage rate and accumulated damage respectively.

Plant dynamic model

The power plant under consideration is a fossil-fueled generating unit having a rated capacity of 525 MWe. The plant dynamics have been represented by a 27th-order nonlinear state-space model, which is described in detail by Weng (1994) and Weng *et al.* (1996). The plant maintains the throttle steam condition at 2415 psia (16.65 MPa) and 950°F (510°C), and the hot reheat steam temperature at 1000°F (537.8°C). The following four valve commands are selected as control inputs: high-pressure turbine governor valve area (AGVR), feedpump turbine control valve area (APTR), furnace fuel/air valve area (AFAR) and reheat spray attemperator valve area (AATR). The measured plant outputs are electric power (JGN), throttle steam temperature (THS), hot reheat steam temperature (THR) and throttle steam pressure (PHS).

Structural damage model

As stated in Section 1, the main theme of this paper is the synthesis of a control system for life extension of the main steam header under different operating conditions of the power plant. The main steam header under consideration is made of SA-213 T22 annealed (2% Cr, 1.25% Mo) steel alloy and has the dimensions of 10 inches (0.254 m) inner diameter and 14 inches (0.356 m) outer diameter. Operating experience in fossil fuel power plants (Creep-Fatigue Pro, 1992) reveals that failure in the main steam header can occur owing to a combination of two forms of damage, namely after progressive thinning of the header wall due to creep/plasticity, and fatigue crack propagation in the radial directions. Progressive thinning of the header wall is caused by thermomechanical loading due to internal (hydrostatic) pressure and high temperature (i.e. close to half the melting point of the material) that induce creep and plastic strain, which is a global phenomenon and occurs throughout the header. In contrast, fatigue crack propagation is a highly localized

form of damage due to mechanical loading in the points of material defects (French, 1993). While defects can be present anywhere in the header wall, the highest stresses start developing at the outer surface over a long period of operation, and therefore fatigue cracks are most likely to begin on the outer surface (Robinson and Swindeman, 1982). To calculate the plastic strain and crack growth, the distribution of time-dependent stress and temperature across the main steam header cross-section is required.

As can be seen in Fig. 2, the component structural model consists of three parts, namely heat transfer, thermoelastic and thermovisco-plastic, where the time-dependent steam temperature, steam pressure and steam flow rate are external inputs generated by the plant model. The damage model in Fig. 2 calculates both damage rate and accumulation as continuous functions of time. The underlying principles for development of the individual models are briefly described below. Details of derivations of the model equations are presented in the Appendix.

The heat-transfer model in Fig. 2 is derived from the classical diffusion equation for heat conduction to calculate the temperature distribution across the header cross-section. Heat flows across the inner boundary of the header cross-section by forced convection and across the outer boundary of the header insulation by

natural convection and radiation. The forcing functions for the heat transfer equations are the steam temperature and steam flow through the header, and the ambient temperature outside the header.

The thermoelastic model in Fig. 2 is formulated on the principle of finite differences to calculate the stresses at discrete nodes along the header cross-section. The model uses a generalized Hooke's law, equilibrium and compatibility conditions and plastic strain relations to arrive at differential equations, with stress being the dependent variable with respect to the spatial variable in the radial direction (Kumar and Mukherjee, 1977). The structural model generates radial, axial and hoop stress at each node.

Plastic strain at each spatial node along the header radius for each instant of time is generated by a unified thermovisco-plastic model of time-dependent creep/plasticity (Freed *et al.*, 1991). The instantaneous plastic strain components at each node are inputs to the thermoelastic model, as seen in the flow diagram of Fig. 2. The model inputs are stress components and temperature at each node, generated by the structural model and the heat transfer model respectively. Tensorial back stress components and the scalar drag stress and limit stress at each node are the internal state

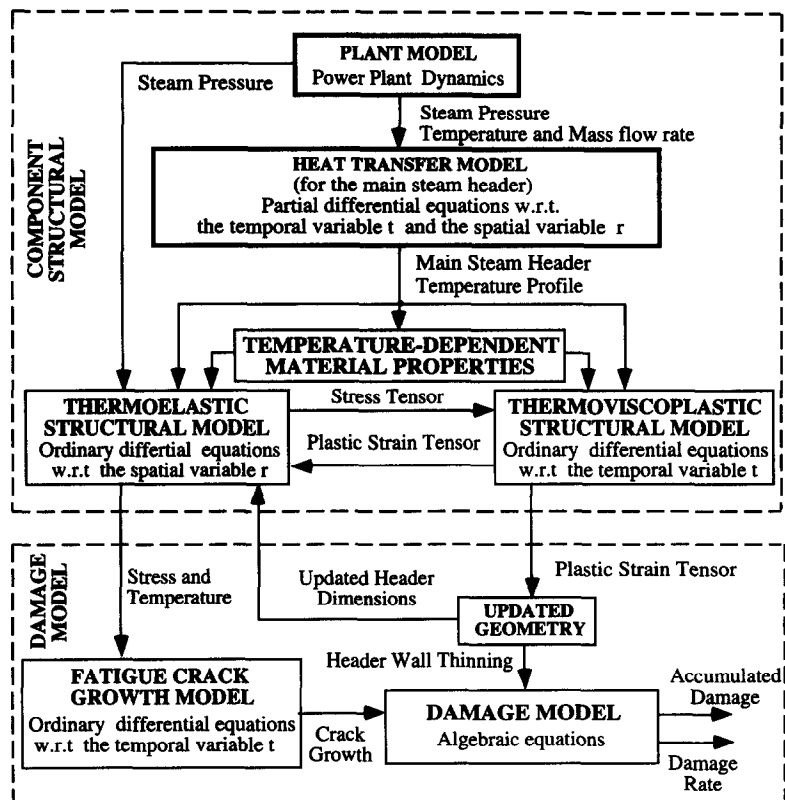


Fig. 2. Flow diagram of the structural damage model.

variables. The thermoviscoplastic model takes into account the effects of dimensional changes due to both rate-dependent creep and rate-independent plasticity. The model equations are in the form of time-dependent ordinary differential equations in the state-variable setting, as described in the Appendix. A major advantage of separating the thermoelastic model from the thermoviscoplastic model is that the derivatives due to the spatial variables are decoupled from those due to the temporal variable.

The thermoviscoplastic model calculates the (irreversible) reduction in the header wall thickness due to plastic strain. The crack growth part of the damage model is based on linear elastic fracture mechanics (LEFM), where the stress intensity factor range ΔK is the key to fatigue crack growth (Suresh, 1991; Anderson, 1994). Austin and Webster (1993) have reported that the LEFM approach can be used for modeling fatigue crack growth phenomena at high temperatures provided that the material crack growth parameters are correctly obtained. The rationale for using the ΔK approach in this application as opposed to ΔJ (Anderson, 1994; Lambert *et al.*, 1988) is relatively mild plasticity and low creep rate of the header material based on the following observations:

- (i) the stress calculations in the component structural model take into account the effects of plastic strain (see the Appendix);
- (ii) the header material partially loses its ductility as it strain-hardens after several stress cycles (Robinson and Swinderman, 1982);
- (iii) the wall temperature, even under transient conditions, is less than half the melting point of the header material;
- (iv) the effects of cavitation crack growth are retarded by dynamic recrystallization because the structural load is at high mean stress with low amplitude (Sklenicka *et al.*, 1993);
- (v) microstructural analysis of cracked header materials (French, 1993) shows the primary mode of fracture to be transgranular, which is in agreement with the LEFM theory.

The crack growth model in Fig. 2 is represented by differential equations with respect to time in the state-variable setting, with time-dependent stress components as inputs (Ray *et al.*, 1994a). As stated earlier in this

section, time-dependent fatigue crack growth rate and crack length are calculated starting from the outer surface of the header. The output of the damage model is a two-dimensional vector whose first element is the reduction in header thickness and whose second element is the time-dependent crack length. Each of the above two elements can be normalized to yield a dimensionless quantity. For example, if the reduction in wall thickness is divided by the original thickness then zero thinning implies virgin condition, and 0.5 thinning implies that the present thickness is half the original thickness. Similarly, the normalized crack damage can be obtained as the ratio of the difference between the current crack length and the initial crack length to the critical crack length (Ray *et al.*, 1994a).

Remark. It follows from the structural damage model presented in the Appendix that fluctuations in the main steam temperature and pressure influence the thermomechanical fatigue and plastic deformation in the header wall. For example, thermal gradients due to large variations in steam temperature may generate high stresses and plastic strain. Similarly, large pressure oscillations produce cyclic stresses, which may result in a large crack growth rate due to an increased stress intensity factor range ΔK . It should be noted that damage dynamics, depicted by (2) above, is a nonlinear and inherently unstable process by its very nature.

3. FEEDFORWARD/FEEDBACK CONTROL SYNTHESIS

The control objective is to manoeuvre the plant from an initial equilibrium state to a new equilibrium state within a specified time and without violating the prescribed physical and damage constraints. The motivation here is to facilitate daily cycling of large electric generating units that were originally designed for baseload operation. A schematic diagram of the life-extending control of a power plant is shown in Fig. 3. The control input U to the plant is composed of the addition of two signals. The first is the feedforward signal U^{ff} and the second is the feedback signal U^{fb} . Prior to initiation of the transients (e.g. load ramp up), U^{ff} is held at the steady-state value of the inputs corresponding to the initial load. During transients, U^{ff} is identically equal to the control policy, which is generated off-line via constrained optimization over a specified finite interval of time. At the expiration of the finite time interval, U^{ff} is held at the steady-state value corresponding to the inputs at the final load. The feedback signal U^{fb}

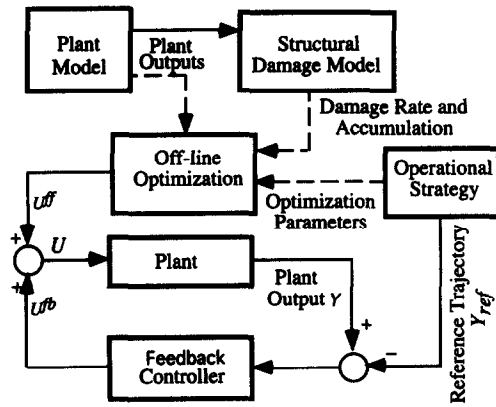


Fig. 3. Structure of the life-extending control system.

is provided on-line by the feedback controller. The purpose of the feedback controller is to track the plant output reference signal specified by the operational strategy module.

The dashed lines in Fig. 3 show the information flow during the off-line optimization. The optimization parameters generated by the operational strategy are

- reference trajectory of the plant outputs Y_{ref} (e.g. load-following trajectory);
- constraints on damage rate, damage accumulation, control inputs and plant outputs;
- weighting matrices used in the cost functional for optimization.

Under steady-state operations, the plant states and inputs are determined by the load and other outputs (pressure and temperatures). Following (1), the steady-state condition is defined as

$$f(x_{ss}, u_{ss}) = 0, \quad y_{ss} = g(x_{ss}, u_{ss}), \quad (5)$$

where the subscript 'ss' indicates the steady state. The steady-state inputs and states are obtained by solving nonlinear algebraic equations (5) for u_{ss} and x_{ss} for a given desired output y_{ss} . Since, in this application, both u_{ss} and y_{ss} are of the same dimension, finding the steady states requires the solution of an algebraic system with an equal number of equations and unknowns. However, even under the steady-state conditions, the damage may continue accumulating because the damage rate in (2) is non-negative. Since u_{ss} and x_{ss} are uniquely determined by y_{ss} in the present problem, the damage and performance are also unique for a given operating condition of load demand, steam pressure and temperature; the role of feedback control (FBC) is to prevent any departure from the desired trajectory arising out of modeling uncertainties and disturbances. On the other hand, damage in power plant components is most severe during transients such as start-up,

shutdown and load-following operations (Creep-Fatigue Pro, 1992), because of rapid fluctuations in steam temperatures, pressures and other state variables. These rapid changes are critical from the points of view of both performance and damage.

Each input of the power plant control system can be changed in different ways to the dual objectives of load following and damage mitigation. An optimal feedforward control (FFC) policy can be generated as an input sequence over a finite-time horizon to enable rapid response to changes in load demand while maintaining the selected plant output variables (e.g. temperature and pressure) within specified bounds and simultaneously minimizing the damage rate and accumulation. Consequently, the performance index is expressed in terms of the deviation from the desired load, deviations of the plant variables from their desired values, and the rate of change of actuator commands. The objective here is to minimize a nonlinear cost functional that represents the plant performance, the damage rate and damage accumulation without violating the specified performance and damage constraints as well as the physical constraints.

The linear feedback system is active during both steady state and transient conditions. Its function is to assure that the plant outputs (i.e. main steam and hot reheat steam temperatures, main steam pressure, and power output) are within specified error bounds, but it is not designed to control damage that is governed by nonlinear differential equations as seen in (2) and the Appendix. Since the tracking error is required to be small in the presence of plant modeling uncertainties, noise, and disturbances entering the control system, the FBC law is designed to achieve robust stability throughout the duration of plant operation in conjunction with FFC. The presence of a feedforward during transient operations reduces the feedback control effort and damage.

Optimal feedforward control synthesis

The optimal feedforward control (FFC) policy is synthesized off-line via constrained nonlinear programming (NP), which is the most general case of mathematical programming where both the cost function and the constraints are allowed to be nonlinear. Optimization of the FFC sequence is a computationally expensive procedure in the present application of wide-range load-following operation. This is mainly due to the fact that the power plant model is nonlinear and of moderately high order (27 states) and the structural damage model is highly nonlinear. For

this reason, on-line methods of optimization, such as receding-horizon predictive control (Mayne and Michalski, 1990), appear to be ineffective for control of damage. Among the existing NP techniques for off-line optimization, the sequential quadratic programming (SQP) method has been shown to outperform many other tested methods in terms of efficiency, accuracy and percentage of successful solutions over a large number of test problems (Wasil *et al.*, 1989). SQP is especially efficient when the evaluation of the cost functional is computationally very expensive (Fletcher, 1987). We have adopted the NPSOL nonlinear programming package (Gill *et al.*, 1986), which is based on the SQP technique, for off-line generation of the optimal FFC policy.

For the above constrained nonlinear programming (NP) problem, the decision variables are the actuator valve positions, which are the control inputs. The quadratic cost functional is chosen to be the sum of the square of weighted ℓ_2 norms of deviation of plant outputs and control effort (change in input valve positions) and weighted ℓ_1 norm of the damage rate and damage accumulation, which are non-negative. The optimization procedure identifies a finite sequence of control inputs $\{u_k\}_{k=0}^{N-1}$ at uniform time steps for $k=0, \dots, N-1$. Since each of the plant and damage models has a continuous-time structure, the control inputs are in effect continuous-time steps where u_k represents the height of the step for the duration $[t_k, t_{k+1})$. The sequence of control inputs are calculated such that the plant can be manoeuvred from a known initial plant state x_0 and damage state v_0 at initial time t_0 close to the specified terminal state and control effort at the final time t_f corresponding to the final time step N . However, there is no guarantee that the plant will actually reach the final state within the finite-time horizon of N steps. The optimization procedure is summarized as follows:

minimize

$$J = \sum_{k=0}^{N-1} (\bar{y}_{k+1}^T Q_{k+1} \bar{y}_{k+1} + \bar{u}_k^T R_k \bar{u}_k + S_k \dot{v}_k) + \sum_{i=1}^l (v_{Ni} - v_{0i}) \quad (6)$$

subject to the following constraints:

$$\begin{aligned} \text{plant dynamics: } x_{k+1} &= x_k + \int_{t_k}^{t_{k+1}} f(x(t), u(t)) dt, \\ x_k |_{k=0} &= x(t_0) = x_0, \end{aligned} \quad (7)$$

$$\text{plant output; } y_k = g(x_k, u_k), \quad (8)$$

$$\text{control-signal bound; } 0 \leq u_k^i < \alpha^i \quad (i = 1, 2, \dots, m), \quad (9)$$

$$\text{plant output constraints: } |\bar{y}_k^i| < \gamma_k^i \quad (i = 1, 2, \dots, p), \quad (10)$$

$$\text{damage rate: } 0 \leq \dot{v}_k^i < \beta_k^i \quad (i = 1, 2, \dots, l), \quad (11)$$

$$\text{damage accumulation: } v_N^i - v_0^i < \Gamma^i \quad (i = 1, 2, \dots, l). \quad (12)$$

Here x_k , u_k and y_k are plant states, control inputs and plant outputs respectively at time t_k , $\bar{y}_k = y_k - \hat{y}_k$ is the deviation of the actual output from the desired output, $\bar{u}_k = u_k - u_{k-1}$ is the incremental change in the control input at time t_k , v_k is the damage state, consisting of creep thinning and fatigue damage states, at time t_k , \dot{v}_k is the damage rate, consisting of creep thinning and fatigue damage rates, at time t_k , N is the total number of discrete time steps for the time period $[t_0, t_f]$, $Q_k \in \mathbb{R}^{p \times p}$, $R_k \in \mathbb{R}^{m \times m}$ and $S_k \in \mathbb{R}^{1 \times l}$ are weighting matrices ($k = 1, \dots, N$), α^i is the normalized upper limit of the i th actuator position vector, β_k^i is the maximum rate of the i th damage state vector at time t_k , γ_k^i is the normalized constraint for the i th output deviation \bar{y}_k^i at time t_k , and Γ^i is the maximum increment of the i th damage state for the time period $[t_0, t_f]$.

Robust feedback control synthesis

The feedback control (FBC) system is designed in the sample-data configuration in which the sampler and hold are synchronized as seen in Fig. 4. That is, even though the computation of the feedback signal $\Delta u(k)$ is completed before expiration of the sampling period, it is held in the buffer until the beginning of the next sample. Although it is possible to apply the feedback signal to the plant input as soon as it is available, synchronization with the sampler makes implementation easier, and should cause very little performance degradation if the sampling period T is chosen small relative to the process dynamics. Having the sampler and hold synchronized allows the use of a powerful sampled-data feedback controller design tech-

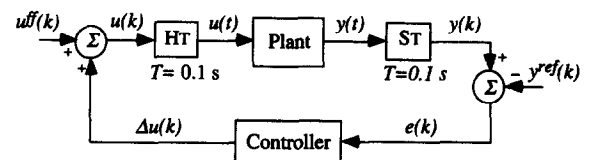


Fig. 4. Feedforward/feedback control system configuration.

nique, which is briefly described below. This design technique takes advantage of the fact that a synchronized sampled-data system is T -periodic since shifting the system inputs by an integer multiple of T will result in the plant outputs being sampled at the same points, but shifted by the multiple of T . Another important issue is that of intersample behaviour. The signal y_k contains information about the signal $y(t)$ only at the sample instants. Measurements of $y(t)$ between these samples are not available to the controller. Discretizing the continuous plant and designing a digital controller based on this discretized plant may result in a design that behaves well at the sample instants, but poorly in between the samples. This becomes especially a problem if T^{-1} is too small with respect to the largest system eigenvalues. For the power plant considered in this paper, a sample time of 0.1 s was found to be sufficient for control purposes.

We have adopted a feedback controller synthesis technique that minimizes the worst-case gain between the energy of exogenous inputs (e.g. noise, disturbances and reference signals) and regulated outputs (e.g. error signals and control effort). This is known as L_2 -induced controller synthesis, which involves finding the stabilizing controller K that minimizes

$$\|T_{zw}(K)\|_{L_2\text{-ind}} = \sup \left\{ \frac{\|z\|_{L_2}}{\|w\|_{L_2}} \mid \|w\|_{L_2} \neq 0 \right\}, \quad (13)$$

where T_{zw} is the closed-loop transfer function between the previously mentioned exogenous inputs w and exogenous outputs z , and $\|\cdot\|_{L_2}$ denotes a norm whose value is the energy of the signal on which it operates. For linear time-invariant systems, controller synthesis based on the induced L_2 norm is known as H_∞ controller synthesis, and has been well documented in the control literature (Doyle *et al.*, 1989). However, H_∞ controller synthesis cannot be applied directly to sampled-data systems because of their time-varying nature. Bamieh and Pearson (1992) proposed a solution to the L_2 -induced controller synthesis problem for sampled-data systems, which has subsequently been incorporated as the function *sdhfsyn* in the MATLAB *mutools* toolbox.

Since the linear model being used for the synthesis of the feedback controller is only an approximation of the true dynamics of the power plant, the designed controller should exhibit robustness properties. The controller should be stable and perform well not only for the nominal linear model, but also for a set of plants of which the actual power plant is assumed to be a member. The reader is referred to Zhou *et al.*

(1996) for a detailed discussion concerning the advantages of including robustness in feedback controller design. Analysis of the robust stability and performance of sampled-data systems has been explored by Sivashankar and Khargonekar (1993). Here they report a ' μ -like' sufficient condition for satisfying robust stability and performance. For controller synthesis, a D - K iteration technique can be used where 'suboptimal' rational polynomial weights D are found using μ -synthesis, and the controller K is found using the induced L_2 sampled-data design procedure. The D s are suboptimal because they are obtained from μ based on the H_∞ norm, which is not equivalent to the induced L_2 norm for sampled-data systems.

Figure 5 shows the setup used for the synthesis of the linear robust controller. The synthesis is based on a linearization of the nonlinear power plant model at a load of 80% of the maximum load. Input multiplicative modeling uncertainty is represented by

$$W_{\text{del}}(s) = 2 \frac{s + 0.05}{s + 1}, \quad (14)$$

which implies that the amount of plant uncertainty is being estimated as being 10% at low frequencies and 200% at high frequencies. The disturbance weighting function is chosen to be

$$W_{\text{dist}}(s) = \frac{0.1}{s + 0.1}, \quad (15)$$

which means that disturbances with frequency content of less than 0.1 rad⁻¹ are expected. In this application, the controller performance is found to be satisfactory, with identical performance weights for the four outputs. In addition, since the control objective is to reduce both low-frequency errors for steady-state performance and large frequency oscillations for damage reduction under transients, the transfer function of the weights must have a large bandwidth. Therefore these weights are chosen to be constant over all frequencies to accommodate the full bandwidth in the operating range of the control system. That is,

$$Wp_i(s) = 35, \quad i = 1, \dots, 4. \quad (16)$$

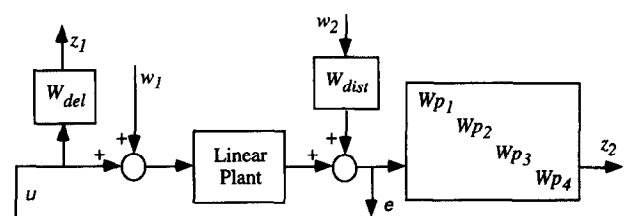


Fig. 5. Synthesis of the linear robust feedback controller.

The MATLAB μ -Analysis and Synthesis Toolbox was used to design a linear feedback controller using the method outlined above. Three D-K iterations were performed where the order of the fits for the D s were chosen to be 4, 3 and 2 respectively. This procedure produced a 63-state robustly stable digital controller. The controller contains such a large number of states because the synthesis method produces a digital controller with the same number of states as the generalized plant. In this case, the generalized plant contains the dynamics of the linear plant model (27 states), the weighting functions (8 states) shown in Fig. 5, extra low-pass filters (4 states) (not shown in Fig. 5) used to make the transfer function from $[w_1, w_2, u]^T$ to $[z_1, z_2, e]^T$ strictly proper (which is required for the sampled-data MATLAB function), and the dynamics of the weighting functions used for the μ -synthesis procedure (i.e. the D s mentioned above) (24 states). Fortunately, most of these states are only lightly controllable and/or observable, and can be safely removed by using standard model-reduction techniques (Zhou *et al.*, 1996). After applying Hankel model reduction to this controller, a 26-state robustly stable controller was obtained that suffered very little performance loss compared with the 63-state controller. To satisfy the robust stability condition, the induced L_2 norm of the transfer function between w_1 and z_1 must be less than 1.0. The stability robustness measure was 0.7683 for the 63-state controller; after order reduction to the 26-state controller, the stability robustness was practically unchanged—the measure increased very slightly to 0.7689. Therefore, in this case, although using this controller design technique resulted in a large-order controller, removal of 37 states made no significant impact on the input–output mapping of the controller.

Implementation of the control system

The implementation of the control system is shown in Fig. 4. Both the feedforward and feedback control signals are discrete signals. The sequence of feedforward commands $u^{ff}(k)$ is stored in a computer a priori, and the signal generated by the feedback controller, $\Delta u(k)$, is calculated by a computer on-line. At each sampling instant (e.g. every 0.1 s), the feedforward and feedback control signals are added together and converted into a continuous signal using a zeroth-order-hold device. Since the feedforward sequence is based on a 1 s sampling time, and the feedback sequence is based on 0.1 s sampling time, each element in the feedforward sequence is applied for 10 consecutive 0.1 s samples. The error signal $e(k)$, which

serves as the input to the feedback controller, is calculated by subtracting samples taken from the plant outputs $y(k)$ from a priori chosen reference trajectory $y^{ref}(k)$. Each of these signals is based on a 0.1 s sampling time.

5. RESULTS OF SIMULATION EXPERIMENTS

Optimal feedforward control policies were obtained for the given plant model and the actuator and plant output constraints for the transient operations of load following. Only the case of power ramp up under normal operating conditions is presented as a typical example in this paper. During the ramp-up operation, the plant load (JGN) was uniformly increased from 40% to 100% base load, i.e. from 210 MWe to 525 MWe, in 360 s. The main steam header pressure (PHS) was constrained within ± 45 psia (± 0.31 MPa) around the nominal value of 2415 psia (16.65 MPa). Similarly, the main steam temperature (THS) was constrained within $\pm 10^\circ\text{F}$ ($\pm 5.56^\circ\text{C}$) around the nominal value of 950°F (510°C), and the hot reheat steam temperature (THR) within $\pm 15^\circ\text{F}$ ($\pm 8.33^\circ\text{C}$) around the nominal value of 1000°F (537.8°).

Before this optimization study was conducted, simulation experiments were conducted for the above ramp-up operation based on an *ad hoc* feedforward input trajectory that is often practiced in industry (Stultz and Kitto, 1992); the objective was to observe the accumulated damage level and damage rate for this power ramping operation. In an *ad hoc* feedforward control, input signals comprised four sequences of control valve positions over the same period of 360 s. The *ad hoc* feedforward input trajectory was constructed by uniformly interpolating between steady-state input values for 40% and 100% load. The control inputs were simply ramped from the initial level to the desired final level in six minutes. The initial and final values of these *ad hoc* feedforward input variables are provided in a previous publication (Weng *et al.*, 1996). The observed damage levels and damage rates were used as constraints during nonlinear optimization to calculate the optimal feedforward trajectory. Values of these constraints are provided later in this section.

The FFC sequence was updated at a uniform interval of 1 s (i.e. $t_k - t_{k-1} = 1$ s for $k = 1, 2, \dots, N$). With four control inputs at each time step, the number of decision variables $\{u_k\}_{k=0}^{N-1}$ is 1440 for a period of 360 s. Since the CPU time required to solve NP problems is approximately proportional to a polynomial function of the number of decision variables, the reduction of the number of decision variables in

the NP formulation is an effective way to circumvent the difficulty of time-intensive computations. Since the desired output trajectory was known, the NP problem was partitioned into a number (M) of (lower-dimensional subproblems. Each of these subproblems was used to optimize the control input sequence for the respective section of the output trajectory. The length of the input sequence (i.e. the number of decision variables) for each subproblem was thus reduced by a factor of M . The complete sequences of (suboptimal) control inputs was formed by concatenating the solutions for each subproblem in the appropriate order. Note that selection of the number M of partitions is a trade-off between suboptimality and computation time. In this application, the feedforward optimization problem was divided into 36 subproblems. That is, each subproblem generated a sequence of length 10. Since there are 4 inputs, each subproblem consists of 40 decision variables. The CPU time for each subproblem is approximately 2 h on a Silicon Graphics Indy, leading up to a total time of 72 h. The specifications for a subproblem are summarized as follows:

- $y_k = [\text{THS}_k, \text{THR}_k, \text{PHS}_k, \text{JGN}_k]^T$ is the output vector;
- $\hat{y}_k = [950^\circ\text{F} \ (510^\circ\text{C}), \ 1000^\circ\text{F} \ (537.8^\circ\text{C}), \ 2415 \text{ psia} \ (16.65 \text{ MPa}), \ Y_{\text{ref}}(k)]$, where $Y_{\text{ref}}(k)$ is the desired power at the specified ramp rate at the instant k ;
- $u_k = [\text{AGV}_k, \text{APT}_k, \text{AFA}_k, \text{AAT}_k]^T$ is the vector of normalized valve positions, varying from 0 (fully closed) to 1 (fully open)

The weighing matrices Q_k and R_k are selected to be diagonal and of size 4×4 . The diagonal elements of each matrix R_k are equal to 10, and $Q_k = \text{diag} (0.0025, 0.001, 0.0001, 0.25)$ for $k = 1, 2, \dots, 8$. In order for the nominal trajectory to reach its desired endpoints more closely, the weights for $k = 9$ and 10 are increased 10 times, i.e. $Q_k = \text{diag} (0.025, 0.01, 0.001, 2.5)$. The choice of weights is governed both by the relative importance of the respective variables and by the absolute value of the output. The weights for the damage rate vector are chosen as: $S_k = [10^6, 10^6]$. Based on the previous mentioned simulation studies with the *ad hoc* trajectory, constraints for creep and fatigue crack damage for each subproblem were selected as follows:

- upper limit of creep thinning rate = $1 \times 10^{-7} \text{ mm s}^{-1}$ or of normalized thinning rate = $2 \times 10^{-9} \text{ s}^{-1}$;
- upper limit of crack growth rate = $2 \times$

$10^{-10} \text{ mm}^{-1} \text{ s}$ or of normalized crack growth rate = $4 \times 10^{-12} \text{ s}^{-1}$;

- upper limit of creep accumulation = $5 \times 10^{-7} \text{ mm}$ or of normalized crack accumulation = 1×10^{-8} ,
- upper limit of crack accumulation = $8 \times 10^{-10} \text{ mm}$ or of normalized crack accumulation = 1.6×10^{-11} .

The values were normalized by dividing them by the initial header wall thickness. The following initial conditions of the damage vector are chosen to represent the midlife state of the header material:

- creep accumulation = $4.5 \times 10^{-2} \text{ mm}$ and fatigue crack accumulation = 1.5 mm.

Upon completion of the optimization task that generated a sequence for each of the four feedforward control inputs, simulation runs were conducted for three different scenarios, each for a midlife operation of the plant for a period of 9000 s. Each of these simulation experiments started with a ramp-up operation. Each ramp-up operation was completed in 360 s (6 min), followed by a steady-state operation around 100% load for 8640 s. In each simulation experiment, during the 100% constant load operation, feedforward inputs were held constant at their respective steady-state values. The simulation runs have two major objectives: first, to demonstrate the superiority of the optimized feedforward trajectory over the *ad hoc* trajectory for both damage mitigation and performance enhancement; second, to demonstrate the role of feedback to maintain performance both during and after the ramp-up operation and further improve upon damage mitigation.

The first scenario used the *ad hoc* input feedforward sequence for the ramp up followed by the steady-state values of the control inputs. Feedback control was used in this simulation. The second scenario used the optimal feedforward control sequences, instead of the *ad hoc* ones, for the ramp-up operation, and maintained the steady-state control inputs for feedforward thereafter. This simulation did not use feedback. The third scenario incorporated the feedback controller in addition to the optimal feedforward inputs used in the second scenario.

Figures 6 and 7 compare the results of closed-loop simulations obtained from the *ad hoc* feedforward control and the optimized feedforward control. Note that feedback control was used in both cases. Figure 6 shows that the overall performance of the optimized feedforward sequence is clearly superior to that of the

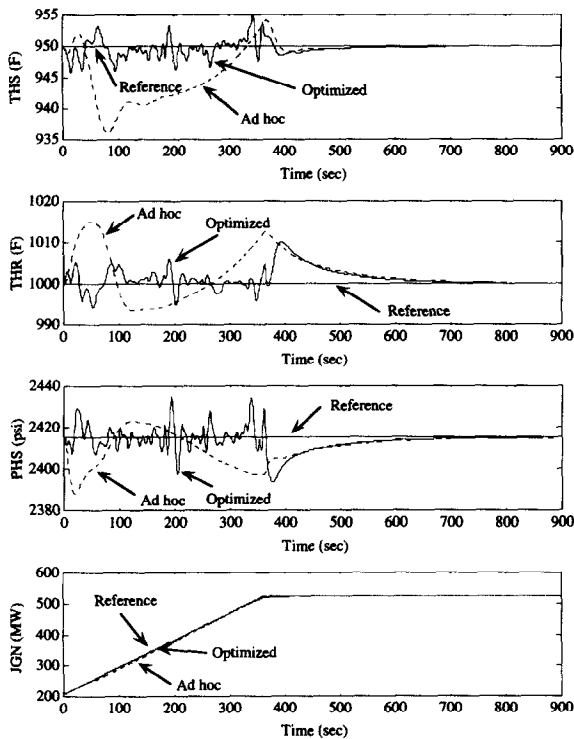


Fig. 6. Performance comparison between *ad hoc* and optimized feedforward.

ad hoc feedforward sequence. The output in the optimized feedforward case follows the reference load (JGN) trajectory more closely. (It is difficult to distinguish the two load trajectories from the plot owing to scaling.) Furthermore, although

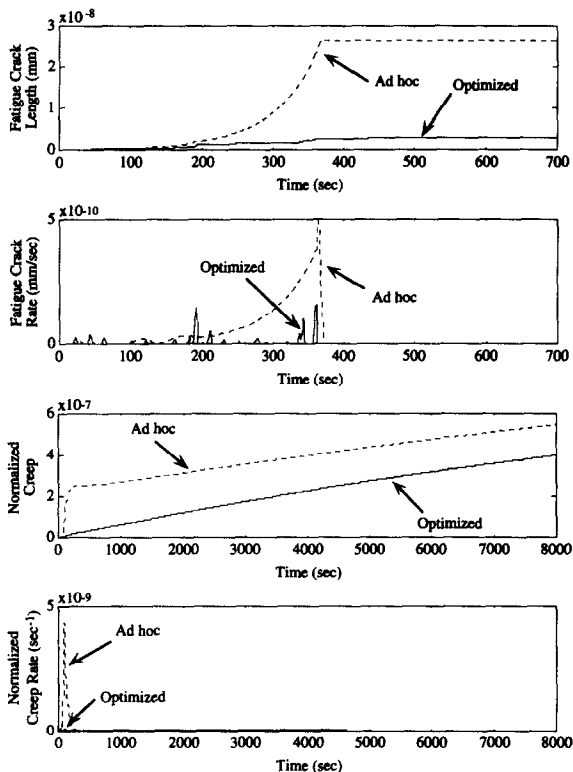


Fig. 7. Damage comparison between *ad hoc* and optimized feedforward.

the temperature and pressure signals in the optimized case have higher-frequency contents due to more rapid manoeuvring of the control valves, they have smaller amplitude than in the *ad hoc* case. For each plant output, steady state is reached at approximately the same time. The optimal trajectory generation is driven by three goals. The first is to follow the output ramp as closely as possible, which is demonstrated in Fig. 6. The second is to keep the three other outputs within specified bounds, for safety reasons and damage mitigation. Therefore it is not necessary to directly limit the frequency contents of the three outputs THS, THR and PHS. However, the outputs need to be kept within the specified bounds. Figure 6 demonstrates that the optimized feedforward keeps the outputs within bounds and relatively closer to the reference output, as compared with the *ad hoc* input. The third aim is to reduce damage due to creep and fatigue in the steam headers. Both creep and fatigue damage are functions of the steam temperature and pressure. The optimization process manipulates these plant variables so that the damage is kept below specified bounds without exceeding the bounds for these outputs, and simultaneously the plant performance is maximized. Therefore the frequency contents of the temperature and pressure outputs are not arbitrary, but are governed by the performance specifications, damage constraints, plant dynamics and the command signal of the power ramp.

Figure 7 compares the damage and damage rates resulting from the plant operation and control scenarios of Fig. 6. Fatigue damage accumulation and rate are calculated by the fatigue crack growth model in terms of the increments of crack length in mm, assuming an initial crack length of 1.5 mm. Creep damage is expressed as a normalized dimensionless variable. It is the reduction in thickness of the header pipe divided by the original thickness. In effect, creep and fatigue damage accumulations and rates shown in Fig. 7 refer to the thinning and cracking of the main steam header. Both fatigue and creep damage are lower for the optimized input as compared with the *ad hoc* input. For both types of damage, under the *ad hoc* feedforward control inputs, the peak occurs during the transient condition of power ramp up. This demonstrates the need for damage mitigation during transient operations. The life-extending control under the optimized feedforward inputs reduces the creep thinning damage by about 40% and the fatigue damage by about 90%, as seen in Fig. 7. The major advantage of the optimal feedforward control over the *ad hoc* feedforward is the significant saving in structural

damage in terms of both fatigue and creep damage. However, this requires rapid maneuvering of the control valves, which will increase wear, and therefore more frequent maintenance of actuator valves will be needed. This is a small price in contrast to the gain achieved by life extension of the steam header and (possibly) other plant components such as steam generators and steam turbines.

Figures 8 and 9 demonstrate the advantages of using feedback control in conjunction with the optimal feedforward control policy. Figure 8 shows that, during the transient operations, the feedback controller tends to bring the output signals closer to the reference signals. However, it is apparent that the feedback controller is especially useful after the optimized part of the feedforward control sequence is over. At this point, the outputs may deviate by a large amount from the desired reference if the feedforward control is used alone, because the plant trajectory may not be within the (possibly narrow) region of attraction of a stable equilibrium point. The feedback controller is able to detect this deviation and adjust the plant input signal in such a way as to lessen this deviation and rapidly bring the outputs to their desired steady state values.

Figure 9 compares the amounts of creep and fatigue damage for the open-loop and closed-loop systems. The performance of the power

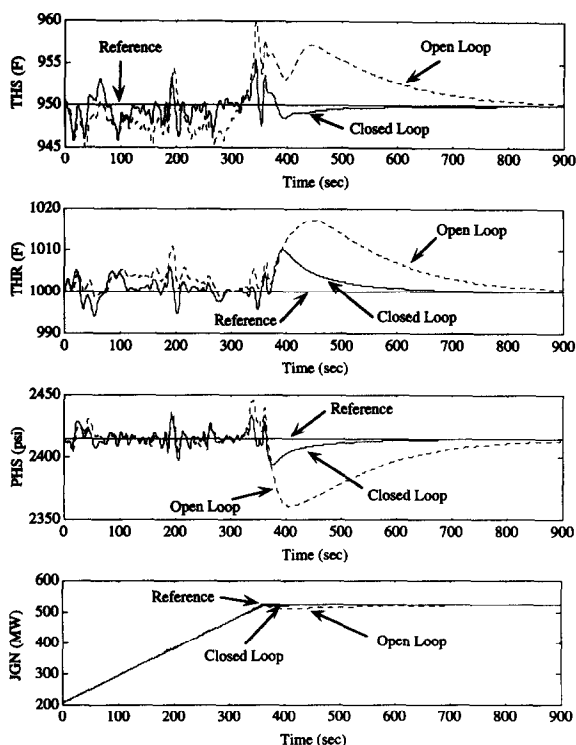


Fig. 8. Performance comparison between open loop and closed loop.

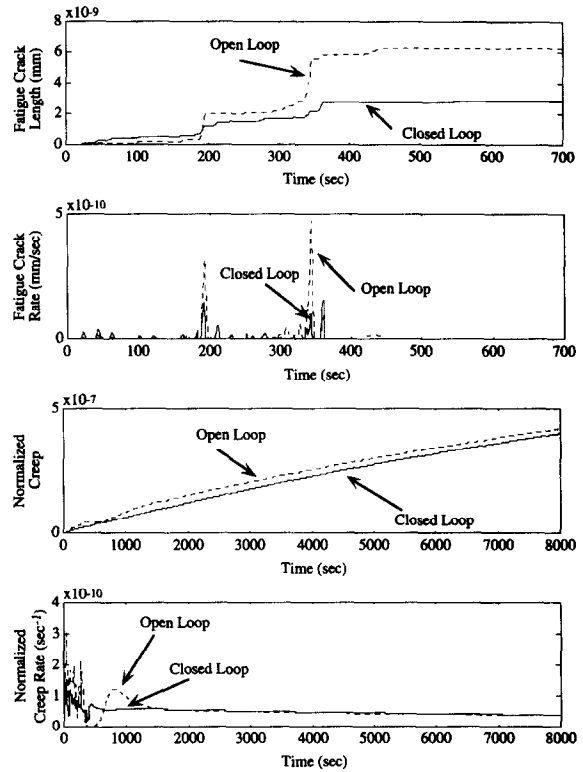


Fig. 9. Damage comparison between open loop and closed loop.

plant is defined as tracking the reference signals for power output and temperatures and pressure. Within this performance definition itself, there is an inherent trade-off. The pride for maintaining the plant load trajectory close to the reference load trajectory of ramp up is a deviation of the steam temperatures and pressure variables from their respective constant reference values and vice versa. During the ramp-up operation, significant improvements in temperature and pressure tracking can be achieved with a marginal sacrifice in power reference signal tracking. This is very encouraging from the perspective of life extension, because the (creep and fatigue) damage in critical plant components is largely driven by temperature and pressure transients. However, we warn against any possible erroneous conclusion that optimal feedforward is not necessary, and feedback along with an *ad hoc* feedforward is adequate. Such a conclusion contradicts the results derived from Figs 6 and 7, where optimal feedforward along with feedback generates much better results than the *ad hoc* feedforward and the feedback. Optimal feedforward is necessary because it gives the feedback controller a trajectory that it can follow with minimal control effort.

The optimal open-loop control sequence is synthesized based on a given nonlinear plant model, which will differ to some degree from the dynamics of the actual power plant. One cause

of the difference is modeling imprecision, and another is the fact that the actual plant dynamics may change with time. To study the effect of plant perturbations on the dynamic performance, the above optimal open-loop and closed-loop simulations were repeated with the following perturbations in the plant parameter.

Inaccuracy in dynamic parameters that do not affect the steady-state response.

- 200% increase in the time constants of the governor, feedpump turbine and fuel/air valves.

Gradual degradation that affects both steady-state and transient responses.

- 5% decrease in the efficiencies of the high-pressure, intermediate-pressure, low-pressure and feedwater pump turbines, and feedwater pumps due to structural degradation of rotating components.
- 5% decrease in the heat-transfer coefficient in the steam generator and reheater tubes resulting from possible scale formation on the inside wall.

Since none of the above parameters change abruptly, the feedback controller will maintain the plant outputs at the desired values under steady-state or quasi-steady-state operating conditions, although the states of the perturbed model will be different from those of the unperturbed model. Therefore, prior to power ramp-up simulation, initial states of the perturbed plant model were set to the steady-state values corresponding to 40% load. The sequence of feedforward control input increments that was generated based on the unperturbed model was applied at the onset of power ramp up. Once the ramping operation is concluded, the feedforward control signal is set to the steady-state value of the perturbed plant model at 100% load for the remainder of the simulation.

Figure 10 shows a comparison between the open-loop and the closed-loop simulation results for the perturbed plant. Obviously, the open-loop sequence that was generated based on the unperturbed model is not very robust when acting alone to control the plant. All four output variables of interest deviate by an unacceptable amount from their desired values, as seen in Fig. 10. When a feedback controller is added, the results are much improved, although they are not nearly as good as the unperturbed case of Fig. 8. The modest success of the feedback controller in manoeuvring the perturbed plant can be attributed to the fact that robustness was

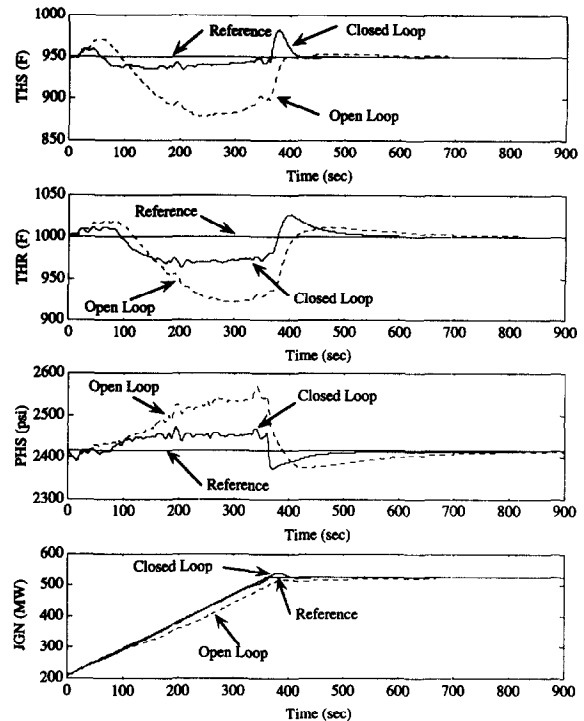


Fig. 10. Performance comparison between open loop and closed loop (perturbed-plant case).

taken into account in the synthesis process. Apparently, it is not possible to synthesize a robust feedforward sequence in a numerically tractable manner.

A comparison between Figs 11 and 9 illustrates that when the feedforward sequence

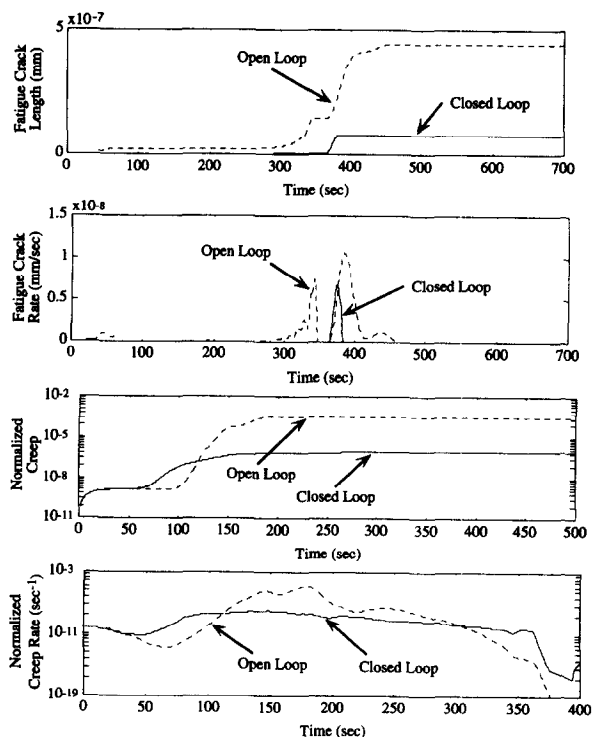


Fig. 11. Damage comparison between open loop and closed loop (perturbed-plant case).

alone acts on the perturbed plant, the damage accumulation becomes much more severe, in contrast to that for the unperturbed model. The fatigue crack length increases by almost two orders of magnitude, and the creep increases by about three orders of magnitude. This drastic increase in damage is caused by the large oscillations in the steam pressure and temperature outputs. For the perturbed simulation, the fatigue damage increment, 9000 s after the start of the ramp, is 4.45×10^{-7} mm for the open-loop case and 8.21×10^{-8} mm for the closed-loop case. Similarly, the creep damage accumulation is 3.12×10^{-4} for the open-loop case and 1.5×10^{-6} for the closed-loop case.

6. SUMMARY, CONCLUSIONS AND FUTURE RESEARCH

This paper has presented the concept and synthesis of life-extending control by creating a feedforward/feedback control policy for enhancement of both dynamic performance and structural durability of fossil fuel power plants. The life-extending control system is capable of rapid manoeuvring of the plant load, in addition to generating crucial diagnostic and maintenance information. For example, the remaining useful life can be predicted to assist maintenance scheduling (Ray and Tangirala, 1996), which is critical for reducing the loss of revenue resulting from unscheduled shutdown and overly conservative operation planning. To this effect, this paper has investigated structural durability of the main steam header under ramp-up operation from 40% to 100% base load. Structural damage in other critical components such as steam generators, turbines and feedwater pumps is being investigated to make the life-extending control system more comprehensive.

The key issue is the trade-off between plant performance and structural durability of critical components. To this effect, a nonlinear constrained optimization procedure has been proposed to generate a finite sequence of feedforward control inputs that must satisfy the physical, operational and damage constraints. A robust sampled-data feedback controller has been synthesized based on an induced L_2 -norm technique. The feedback controller minimizes undesirable effects, such as poor performance and increased damage, due to exogenous disturbances and plant modeling errors. Computer simulations demonstrate that both high performance and low damage can be attained using the proposed feedforward/feedback architecture.

This concept of life-extending control, based on characterization of material properties, can be used for any other processes where structural durability is a critical issue. This concept has been used for control of rocket engines (Dai and Ray, 1995), and is currently being applied to aircraft engines. It can also be used for performance, life enhancement, maintenance and diagnostics for other mechanical systems, such as automotive engines and continuous-time production processes (Ray *et al.*, 1994a, b). Modeling of damage in these components and generalization of the optimal feedforward control policy are topics of future research. Additional constraints (e.g. those due to pollutant emission in fossil fuel plants) may also be included in the optimization procedure.

Acknowledgements—The work presented in this paper has been supported by the National Science Foundation under Grants ECS-9216386, DMI-9424587 and CMS-9531835, and the Electric Power Research Institute under Contract EPRI RP8030-05.

REFERENCES

- Anderson, T. L. (1994) *Fracture Mechanics: Fundamentals and Applications*, 2nd ed. CRC Press, Boca Raton, FL.
- Austin, T. S. P. and Webster, G. A. (1993) Application of a creep-fatigue crack growth model to Type 316 stainless steel. In *Behavior of Defects at High Temperatures*, pp. 219–238. European Structural Integrity Society, Vol. 15, Sheffield, U.K.
- Bamieh, B. A. and Pearson, J. B. Jr. (1992) A general framework for linear periodic systems with applications to H_2 sampled-data control. *IEEE Trans. Autom. Control*, **AC-37**, 418–435.
- Bannantine, J. A., Comer, J. J. and Handrock, J. L. (1990) *Fundamentals of Metal Fatigue Analysis*. Prentice-Hall, Englewood Cliffs, NJ.
- Brussat, T. R. (1971) An approach to predicting the growth to failure of fatigue cracks subjected to arbitrary uniaxial cyclic loading. In *Damage Tolerance in Aircraft Structures*, ASTM STP 486, pp. 122–143. American Society for Testing and Materials, Philadelphia.
- Creep-Fatigue Pro (1992) *Creep-Fatigue Pro: On Line Creep-fatigue Damage and Crack Growth Monitoring System*. EPRI TR 100907, Project 1893-11, Final Report, July, Structural Integrity Associates, San Jose, CA.
- Dai, X. and Ray, A. (1995) Life prediction of the thrust chamber wall of a reusable rocket engine. *AIAA J. Propulsion, and Power* **11**, 1279–1287.
- Doyle, J. C., Glover, K., Khargonekar, P. P. and Francis, B. A. (1989) State-space solutions to standard H_2 and H_∞ control problems. *IEEE Trans. Autom. Control* **AC-34**, 831–847.
- Fletcher, R. (1987) *Practical Methods of Optimization*, 2nd ed. Wiley, Chichester.
- Freed, A. D., Chaboche, J. L. and Walker, K. P. (1991) A viscoplastic theory with thermodynamic considerations. *Acta Mech.* **90**, 155–174.
- French, D. N. (1993) *Metallurgical Failures in Fossil Fired Boilers*, 2nd ed. Wiley-Interscience, New York.
- Gill, P. E., Murray, W., Saunders, M. A. and Wright, M. H. (1986) *User's Guide for NPSOL (Version 4.0): A Fortran Package for Nonlinear Programming*. Stanford University.
- Kumar, V. and Mukherjee, S. (1977) Creep analysis of metallic structures in the presence of thermal gradients using newer constitutive relations. *ASME J. Press. Vessel Technol.* **99**, 272–281.

- Lambert, Y., Saillard, P. and Bathias, C. (1988) Application of the J concept to fatigue crack growth in large-scale yielding. In *Fracture Mechanics: 19th Symp. ASTM STP 969*, Philadelphia, PA, pp. 318–329.
- Mayne, D. Q. and Michalski, H. (1990) Receding horizon control of nonlinear systems. *IEEE Trans. Autom. Control AC-35*, 814–824.
- Newman, J. C. and Raju, I. S. (1984) Stress-intensity factor equations for cracks in three-dimensional finite bodies subjected to tension and bending loads. *NASA Tech. Memo. 2845*, NASA Lewis Research Center, Cleveland, OH.
- Ray, A. and Tangirala, S. (1996) Stochastic modeling of fatigue crack dynamics for on-line damage estimation and life prediction. *IEEE Trans. Control Syst. Technol. CST-4*, 443–451.
- Ray, A., Wu, M.-K., Carpino, M. and Lorenzo, C. F. (1994a) Damage-mitigating control of mechanical systems: Part I—Conceptual development and model formulation. *ASME J. Dyn. Syst. Meas., Control* **116**, 437–447.
- Ray, A., Wu, M.-K., Carpino, M. and Lorenzo, C. F. (1994b) Damage-mitigating control of mechanical systems: Part II—Formulation of an optimal policy and simulation. *ASME J. Dyn. Syst., Meas., Control* **116**, pp. 448–455.
- Robinson, D. N. and Swindenman, R. W. (1982) Unified creep-plasticity constitutive equations for 2-1/4 Cr-1 Mo steel at elevated temperature. Oak Ridge National Laboratory, Oak Ridge, Tennessee, Contract No. W-7405-Eng-26.
- Sklenicka, V., Lukas, P. and Kunz, L. (1993) On the role of cavitation in creep/high-cycle fatigue fracture. In *Behavior of Defects at High Temperatures*, pp. 27–46. European Structural Integrity Society, Vol. 15, Sheffield, U.K.
- Sivashankar, N. and Khargonekar, P. P. (1993) Robust stability and performance analysis of sampled-data systems. *IEEE Trans. Autom. Control AC-38*, 58–69.
- Stultz, S. C. and Kitto, J. B., eds (1992) *Steam/Its Generation and Use*, 40th ed. Babcock & Wilcox, Barberton, OH.
- Suresh, S. (1991) *Fatigue of Materials*. Cambridge University Press.
- Wasil, E., Golden, B. and Liu, L. (1989) State-of-the-art in nonlinear optimization, software for the microcomputer. *Comput. Oper. Res.* **6**, 497–512.
- Weng, C.-K. (1994) Robust wide range control of electric power plants. PhD dissertation, Pennsylvania State University.
- Weng, C.-K. and Ray, A. (1997) Robust wide range control of steam-electric power plants. *IEEE Trans. Control Syst. Technol. CST-5*, 74–88.
- Weng, C.-K., Ray, A. and Dai, X. (1996) Modelling of power plant dynamics and uncertainties for robust control synthesis. *Appl. Math. Modelling* **20**, 501–512.
- Vidyasagar, M. (1992) *Nonlinear Systems Analysis*, 2nd ed. Prentice-Hall, Englewood Cliffs, NJ.
- Zhou, K., Doyle, J. C. and Glover, K. (1996) *Robust and Optimal Control*. Prentice-Hall, Upper Saddle River, NJ.

APPENDIX A—GOVERNING EQUATIONS OF THE STRUCTURAL DAMAGE MODEL

Figure 2 in the main body of the paper describes the functional relationships between different parts of the structural damage model. This appendix presents the details of modeling creep plasticity and crack growth phenomena in the main steam header of fossil fuel power plants. The heat-transfer model is discussed first, followed by the stress-strain model, which contains the thermoviscoplastic and thermoelastic models. The final two sections discuss the crack growth model and the damage model. Unless otherwise stated, the following nomenclature is used in the sequel:

- t = time, the independent temporal variable;
- r = radius, the independent spatial variable;
- θ = the circumferential or hoop direction;
- z = the axial direction.

A.1. Heat-transfer model

Heat transfer from steam to the inner wall of the header takes place owing to forced convection through the header wall and insulation due to conduction and from the insulation to the ambient atmosphere by free convection and radiation. The following major assumptions are made in the heat-transfer model:

- the temperature drop along the length of the pipe is assumed to be negligible;
- the header is radially symmetrical, resulting in one-dimensional heat flow in the radial direction;
- forced convection causes heat flow from steam to the header because of high Reynolds number (note that the steam velocity is in the range of 40–100 m s⁻¹);
- there is no air cushion between the header surface and the insulation.

The one-dimensional, time-dependent heat-conduction equation in cylindrical coordinates is

$$\rho C_p \frac{\partial T(r, t)}{\partial t} = \frac{1}{r} \frac{\partial}{\partial r} \left(rk \frac{\partial T}{\partial r} \right) + q, \quad (\text{A.1})$$

where ρ is the density of the main steam header material, C_p is the specific heat of the main steam header material, T is the temperature, which is a function of time and radial distance from the pipe center, k is the thermal conductivity of the main steam header material, and q is the heat generated per unit volume in the main steam header material. In this case, $q = 0$, since no heat is generated inside the main steam header material. On rearranging, (A.1) can be rewritten as

$$\frac{1}{\alpha} \frac{\partial T(r, t)}{\partial t} = \frac{1}{r} \frac{\partial}{\partial r} \left(r \frac{\partial T}{\partial r} \right), \quad (\text{A.2})$$

where $\alpha = k/\rho C_p$ is the thermal diffusivity of the main steam header material.

Since (A.2) cannot be solved analytically, since the temperature varies with both position and time, a numerical method is necessary to solve for the temperature profile. The geometry and boundary conditions involved in this problem are simple. Therefore the finite-difference approach appears to be an appropriate choice. After (A.2) has been rearranged as

$$\frac{1}{\alpha} \frac{\partial T}{\partial t} = \frac{\partial^2 T}{\partial r^2} + \frac{1}{r} \frac{\partial T}{\partial r}, \quad (\text{A.3})$$

the spatial derivative is discretized at the n th instant via central differencing:

$$\left. \frac{\partial^2 T}{\partial r^2} \right|_{i,n} = \frac{T_{i+1}^n - 2T_i^n + T_{i-1}^n}{(\Delta r)^2}, \quad (\text{A.4})$$

where n indicates the time step while $i-1$, i and $i+1$ indicate the spatial locations of the nodes, and

$$\left. \frac{1}{r} \frac{\partial T}{\partial r} \right|_{i,n} = \frac{1}{r_i} \frac{T_{i+1}^n - T_{i-1}^n}{2(\Delta r_i)}. \quad (\text{A.5})$$

If M spatial nodes are selected in the discretized model then there are M equations with $M+2$ unknowns. The two additional equations are obtained from the boundary conditions at the inner and outer radii. The boundary condition at the inner radius is governed by the forced-convection heat-transfer equation, and that at the outer radius by the free-convection and radiation heat-

transfer equations. Once the spatial derivatives have been calculated, the problem is reduced to an initial-value problem in the time domain. The variable-step Runge–Kuta method was adopted after examining different explicit and implicit techniques.

A.2. Thermoviscoplastic model

A (nonlinear) thermoviscoplastic model (Freed *et al.*, 1991) that takes into account the combined effects of creep and plasticity under time-dependent stress and temperature conditions has been used to calculate the inelastic strain in the material. Stress and temperature are the inputs in the Freed model, and the internal state variables include tensorial plastic strain ε_{ij}^p , anisotropic tensorial back-stress flux β_{ij} , isotropic scalar drag stress flux δ and isotropic scalar limit stress flux λ . While back stress is a dynamic recovery term arising owing to kinematic strain hardening, drag stress and limit stress are static recovery terms arising owing to isotropic strain hardening. At the initial condition, the material is usually annealed, and $\beta(0) = 0$. As β evolves, the material develops a flow-induced anisotropy. The initial values of δ and λ depend on the material and its heat treatment.

This unified thermoviscoplastic model takes into account the combined effects of rate-dependent creep and rate-independent plasticity. The following major assumptions are made in the thermoviscoplastic model:

- the temperature, stress, and strain distributions in the header wall are radially symmetrical;
- the total strain $\varepsilon^{\text{total}}$ is assumed to be the sum of elastic, plastic and thermal strains ε^e , ε^p and ε^{th} respectively. That is,

$$\varepsilon_{ij}^{\text{total}}(r, t) = \varepsilon_{ij}^e(r, t) + \varepsilon_{ij}^p(r, t) + \varepsilon_{ij}^{\text{th}}(r, t), \quad i, j = r, \theta, z; \quad (\text{A.6})$$

- the dynamic and static recovery terms are uncoupled.

The deviatoric stress S_{ij} and the effective stress Σ_{ij} at any point in the pipe are defined in terms of the stress tensor σ_{ij} as follows:

$$S_{ij} = \sigma_{ij} - \frac{1}{3}\sigma_{kk}\delta_{ij}, \quad \Sigma_{ij} = S_{ij} - B_{ij}, \quad (\text{A.7})$$

where δ_{ij} is the Kronecker delta and $B_{ij} = H_b\beta_{ij}$.

Flow law. The plastic strain-rate relations are

$$\dot{\varepsilon}_{ij}^p = \Theta Z \frac{\Sigma_{ij}}{\|\Sigma\|_2}, \quad (\text{A.8})$$

where $\|\Sigma\|_2 = \sqrt{\frac{2}{3}\Sigma_{ij}\Sigma_{ij}}$ is the ℓ_2 -norm of the effective stress tensor. The thermal-diffusivity function Θ and Zener–Hollomon parameter are defined as

$$\Theta = \begin{cases} \exp(-Q/kT) & (T \geq \frac{1}{2}T_m), \\ \exp\left\{\frac{-2Q}{kT_m}\left[\ln\left(\frac{T_m}{2T}\right) + 1\right]\right\} & (T \leq \frac{1}{2}T_m), \end{cases} \quad (\text{A.9})$$

$$Z(F) = \begin{cases} AF^n & (F \leq 1), \\ A \exp[n(F-1)] & (F \geq 1), \end{cases} \quad (\text{A.10})$$

where Q is the activation energy, k is Boltzmann's constant, T is the absolute temperature, T_m is the melting point of the material, A and n are material constants based on the steady-state creep-flow properties, and the function F is defined as $F = \|\Sigma\|_2/D$, $D = H_d\delta$.

Evolutionary laws. The governing equations for the internal state variables, namely the back stress β_{ij} and the drag stress δ , are

$$\dot{\beta}_{ij} = \dot{\varepsilon}_{ij}^p - \frac{H_b\beta_{ij}}{H_r\lambda} \|\dot{\varepsilon}_{ij}^p\|_2, \quad (\text{A.11})$$

$$\dot{\delta} = \frac{1}{G} [\|\dot{\varepsilon}_{ij}^p\|_2 - \Theta R(G)] = \frac{1}{G} \left[1 - \frac{R(G)}{Z(F)}\right] \|\dot{\varepsilon}_{ij}^p\|_2, \quad (\text{A.12})$$

$$\dot{\lambda} = \frac{H_d\delta}{H_r\lambda} (F - G)\dot{\varepsilon}_{ij}^p = \left[\frac{\|\Sigma\|_2}{H_r\lambda} - \frac{H_d\delta}{\bar{C} - H_d\delta}\right] \|\dot{\varepsilon}_{ij}^p\|_2, \quad (\text{A.13})$$

and the thermal recovery function R is defined as

$$R(G) = \begin{cases} AG^n & (G \leq 1), \\ A \exp[n(G-1)] & (G \geq 1), \end{cases} \quad (\text{A.14})$$

$$G = \frac{H_r\lambda}{\bar{C} - H_d\delta},$$

where \bar{C} , H_b , H_d and H_r are scalar positive-valued inelastic material constants. The state equations use effective stress as the forcing function, which in turn is a function of the stress tensor. For the header, all shear stresses are zero, i.e. the circumferential, radial and axial stress are the only non-zero stresses. The governing equations also need temperature and initial values of the four state variables ε^p , β , δ and λ . Once these values are fed to the thermoviscoplastic model, it calculates the time derivative for each state. The derivatives are integrated using numerical techniques, similar to that used for the heat-transfer model, to recursively obtain the state variables.

A.3. Thermoelastic model

The thermoelastic model is used to determine the stresses in the main steam header wall under non-isothermal conditions. The model is a finite-difference model in the cylindrical coordinates, which is constructed by partitioning the header cross-section into concentric rings and then calculating the stresses at each ring boundary. The following major assumptions are made in the thermoelastic model.

- The only force acting on the header is due to internal hydrostatic pressure of steam.
- Body forces (e.g. due to gravity) are negligible compared to the surface forces due to hydrostatic steam pressure.
- The header is radially symmetrical, implying that, in cylindrical coordinates, stress is independent of the circumferential direction coordinate.
- Plane sections remain plane and parallel to each other, implying the concept of generalized plane strain.
- Pressure and temperature drop along the header length are negligible, implying that stress at any point in the header wall is not a function of the axial direction.
- The header is supported at the ends by expandable joints that do not offer resistance to expansion, implying that the axial direction is force-free. However, generalized plane strain implies that the axial direction is not stress-free.
- There are no shear stresses in the header walls.
- Owing to the radial symmetry, displacements in the circumferential direction are zero.
- The vibratory motion of the header is negligible because of the absence of bending and torsion of the header.

The above assumptions reduce the stress tensor to three normal stresses in the radial (r), circumferential (θ) and axial (z) directions, which are functions of radial distance r and time t . Note that the stress in the axial direction is also a function of r and t , even though the force in the axial direction is assumed to be zero.

Quasistatic force equilibrium in the radial direction yields the following partial differential equation:

$$\frac{\partial \sigma_r}{\partial r} + \frac{\sigma_r - \sigma_\theta}{r} = 0, \quad (\text{A.15})$$

where r is the radial coordinate, σ_r is the normal stress in the radial direction, and σ_θ is the normal stress in the circumferential direction.

Force equilibrium in the axial direction yields

$$\int_A \sigma_z(r) dA = 0 \quad (\text{A.16})$$

where σ_z is the stress in the axial direction, A is the cross-sectional area and dA is the differential cross-sectional

area. The stress–elastic-strain relations from the generalized Hooke's law are

$$\begin{aligned}\varepsilon_r &= \frac{1}{E} [\sigma_r - \nu(\sigma_\theta + \sigma_z)], \\ \varepsilon_\theta &= \frac{1}{E} [\sigma_\theta - \nu(\sigma_r + \sigma_z)], \\ \varepsilon_z &= \frac{1}{E} [\delta_z - \nu(\sigma_r + \sigma_\theta)],\end{aligned}\quad (\text{A.17})$$

where E is the modulus of elasticity and ν is Poisson's ratio. Since the total strain in the axial direction has been assumed to be constant throughout the pipe, i.e.

$$\varepsilon_z^{\text{total}} = \bar{C}, \quad (\text{A.18})$$

the strain–displacement relations for the radial and hoop directions are;

$$\frac{\partial u}{\partial r} = \varepsilon_r^{\text{total}}, \quad \frac{u}{r} = \varepsilon_\theta^{\text{total}}. \quad (\text{A.19})$$

As can be seen from the interactions of the thermoelastic and thermoviscoplastic models in Fig. 2, the stress is obtained from the thermoelastic model and the plastic strain from the thermoviscoplastic model. There are a total of 17 unknowns, which are the three normal-direction components for each of stress, elastic strain, plastic strain, thermal strain and total strain as well as displacement u in the radial direction and the constant \bar{C} in (A.18). The heat-transfer model described in Section A.1 provides three equations for the three thermal strains, based on the temperature distribution. The thermoviscoplastic model described in Section A.2 provides a total of six equations for three plastic strains and three total strains. The remaining 8 equations are obtained from (A.15)–(A.19). Thus all 17 unknowns are accounted for. Solution of this set of equations yields the following equations for the stress and \bar{C} :

$$\begin{aligned}r^2 \frac{\partial^2 \sigma_r}{\partial r^2} + 3r \frac{\partial \sigma_r}{\partial r} &= \frac{E}{1-\nu^2} \left(\varepsilon_r^p - \varepsilon_\theta^p - r \frac{\partial \varepsilon_\theta^p}{\partial r} \right. \\ &\quad \left. - r \frac{\partial \varepsilon_\theta^{\text{th}}}{\partial r} + \nu r \frac{\partial \varepsilon_z^p}{\partial r} - \nu r \frac{\partial \varepsilon_z^{\text{th}}}{\partial r} \right),\end{aligned}\quad (\text{A.20})$$

$$\begin{aligned}\sigma_\theta &= r \frac{\partial \sigma_r}{\partial r} + \sigma_r, \\ \bar{C} &= \int [E(\varepsilon_r^p + \varepsilon_z^{\text{th}}) - \nu(\sigma_r + \sigma_\theta)] \frac{dA}{EA}\end{aligned}\quad (\text{A.21})$$

$$\sigma_z = E(\bar{C} - \varepsilon_z^p - \varepsilon_z^{\text{th}}) + \nu(\sigma_r + \sigma_\theta), \quad (\text{A.22})$$

with the following boundary conditions:

$$\begin{aligned}\sigma_r &= -p \quad \text{at } r = \text{inner radius}, \\ \sigma_r &= 0 \quad \text{at } r = \text{outer radius},\end{aligned}\quad (\text{A.23})$$

where p is the hydrostatic pressure of steam inside the header. Similarly to what was done in the heat-transfer model, (A.20) is solved numerically by partitioning the header cross-section into concentric circles, and the spatial derivatives are calculated using the central difference technique. This reduces the partial differential equation (A.20) into a system of algebraic equations. The results of (A.20) are used to solve (A.21) and (A.22).

A.4. Crack growth model

The crack growth model is built upon the concept of linear elastic fracture mechanics (LEFM). The fracture behavior of a linear elastic structure can be characterized by stress intensity factor K , which is given by

$$K = C\sigma\sqrt{\pi a}, \quad (\text{A.24})$$

where C is a dimensionless geometric correction factor, σ is the far-field applied stress and a is a characteristic crack dimension. The fatigue crack process is assumed to belong to Mode I, where the principal load, applied to the crack plane, is normal to the crack surface and tends to open the crack

(Bannantine *et al.*, 1990; Anderson, 1994). The influence coefficient approach (Newman and Raju, 1984) is used to account for the non-uniform stress in the main steam header. In this method, remote stress normal to the crack plane (Mode I) is represented by a cubic equation as

$$\sigma_{\text{normal}} = A_0 + A_1x + A_2x^2 + A_3x^3 = \sum_{j=0}^3 A_jx^j, \quad (\text{A.25})$$

where x is the distance measured from the crack tip along the crack. The dimensionless stress distribution is given by

$$\sigma_j = \left(\frac{x}{a}\right)^j \quad \text{for } j = 0, \dots, 3. \quad (\text{A.26})$$

Note that only normal stresses acting in the range $0 \leq x \leq a$ need to be considered, because stresses at $x > a$ do not contribute to the stress intensity factor K .

Equation (A.25) can be rewritten in the form

$$\sigma_{\text{normal}} = \sum_{j=0}^3 A_j a^j \left(\frac{x}{a}\right)^j. \quad (\text{A.27})$$

For semi-elliptic cracks, the stress intensity factor in the cubic polynomial stress distribution of (A.27) is given by Anderson (1994) as

$$K = \sqrt{\frac{\pi a}{Q}} \sum_{j=0}^3 G_j A_j a^j, \quad (\text{A.28})$$

where Q is the crack shape parameter, which is a function of a and c ; the G_j are pre-determined influence coefficients, which are given by Anderson (1994) as functions of cylinder dimensions, crack shape and crack dimensions.

Remark. Equation (A.28) is a modification of (A.24) where $C \equiv 1/\sqrt{Q}$ and $\sigma \equiv \sum_{j=0}^3 G_j A_j a^j$.

The load history in this application is of varying amplitude, where the effects of crack retardation/acceleration must be considered. Therefore the crack closure model, which is an extension of the Paris model (Bannantine *et al.*, 1990), is adopted here. It assumes that residual displacements in the wake of a crack cause crack faces to contact or close before the tensile load is removed. This model predicts crack retardation in a high-to-low loading sequence and acceleration in low-to-high loading. The cracks open only if the applied stress is greater than the crack opening stress σ_{op} , which depends on the loading history. To this effect, the stress intensity factor range is calculated as

$$\Delta K_{\text{eff}} = K_{\text{max}} - K_{\text{op}}, \quad (\text{A.29})$$

where K_{max} and K_{op} are calculated using the maximum stress σ_{max} and the crack opening stress σ_{op} , following (A.28). The modified Paris equation is

$$\left(\frac{da}{dN}\right)_i = C_0 (\Delta K_{\text{eff}})_i^m, \quad (\text{A.30})$$

where i corresponds to the i th cyclic; C_0 and ΔK_{eff} correspond to the same closure level, and are defined as

$$C_0 = \frac{C}{U^m}, \quad U = \frac{\Delta K_{\text{eff}}}{\Delta K}. \quad (\text{A.31})$$

$\Delta K = K_{\text{max}} - K_{\text{min}}$, and K_{max} and K_{min} are calculated from the maximum stress σ_{max} and the minimum stress σ_{min} following (A.28).

The computation-intensive calculations of ΔK_{eff} from σ_{op} can be simplified by the block loading approach (Brussat, 1971) if the crack growth during any given loading block is not large enough to grow out of the plastic zone. Blocks can be created if there is no very large overload followed by constant-amplitude load cycles; and if the stress amplitude is small compared with the mean stress ratio for each cycle

within the blocks, it is assumed that

$$\sigma_{op} = \sigma_{min} \quad \text{if } \sigma_{min} > 0, \quad (\text{A.32})$$

which is the case for the steam header under consideration. This assumption allows calculation of crack growth per cycle by first calculating K_{max} and K_{op} , and then using (A.31) and (A.30) to evaluate the crack growth per cycle in a block. The crack growth equation is then transformed into a differential equation following the procedure of Ray *et al.* (1994a).

A.5. Computation of damage rate and accumulation

The damage vector in the main steam header has two components, namely wall thinning and fatigue crack. The overall wall thinning occurs owing to global creep deformation in the header. Experience reveals that crack growth takes place on the outer surface of the header (Robinson and Swindeman, 1982). Crack growth occurs in the radial direction, and is driven by circumferential stress. Over an extended period of use, the inner surface becomes softer, and crack propagation begins on the outer surface. The thickness at each instance is calculated along with

thinning damage as follows:

$$\begin{aligned} t_f &= R_f^{out} - R_f^{in}, & t_i &= R_i^{out} - R_i^{in}, \\ R_f^{out} &= R_i^{out}(1 + \epsilon_\theta^{out}), & R_f^{in} &= R_i^{in}(1 + \epsilon_\theta^{in}), \end{aligned} \quad (\text{A.33})$$

$$\text{thinning damage} = \frac{t_i - t_f}{t_i},$$

where t is the header wall thickness, R is the radius, ϵ_θ is the plastic strain in the circumferential direction, the subscripts 'i' and 'f' indicate the initial and present conditions respectively and the superscripts 'out' and 'in' initiate outer and inner surfaces of the header respectively.

The second element will be overall crack length. The value of the crack growth rate is given directly by the crack growth model. However, this calculation is done as crack growth per cycle. To convert it from a load-cycle-based calculation to a time-based calculation, the following formula is used:

$$\frac{da}{dt} = \frac{da}{dN} \frac{dN}{dt}. \quad (\text{A.34})$$

The crack length is calculated by integrating this growth rate numerically.